Original article

Impact of four different CO_2 injection schemes on extent of reservoir pressure and saturation

Harpreet Singh*

National Energy Technology Laboratory, Morgantown, West Virginia, USA

Abstract:
This study investigates how four different injection schemes, (i. constant rate, ii. stepwise increasing rate, iii. stepwise decreasing rate, and iv. cyclic rate), constrained by the cumulative amount of CO_2 injected, affect the likely extent of pressure buildup and CO_2 plume, which play a role in the appraisal of environmental risk performance at CO_2 storage sites. This objective is achieved using a representative model of a realistic site consisting of multi-layer sandstone that is extremely permeable (between 1 to 2 Darcy) and separated by thin layers of shale extending laterally with sporadic discontinuities in form of perforations.

Results show that cyclic injection tends to keep the pore pressure lower than the other three injection schemes, while the highest pressure increase over the entire injection period (50 years) is observed with stepwise decreasing rate. The compressibility of CO_2 plays a role in attenuating the impact of fluctuating cyclic injection signals on pressure after 30 years of injection, where this time decreases by 5 years in case of heterogeneous scenario. Except for the cyclic injection scheme, all other three injection schemes lead to almost the same magnitude and areal extent of CO_2 saturation, while it shows a cyclic behavior in the case of the cyclic injection. Major observations are similar in both homogeneous and heterogeneous scenarios, although layered heterogeneity in the representative site introduces small differences in results.

The results imply that it would be preferable to store CO_2 using a cyclic injection scheme in storage reservoirs that may be prone to high pressure buildup during injection because of their geology (e.g. fractured shale reservoirs). These results also carry important implications for enhanced oil recovery (EOR) using CO_2 where the primary goal is to drive the oil out by increasing pore pressure; for EOR by CO_2, stepwise decreasing rate would be most preferable as it leads to highest increase in pore pressure.

1. Introduction

The increasing production of carbon dioxide (CO_2) at industrial scale either from energy (from fossil fuels, bio-renewable sources, etc.) or other industrial sources will required to be decarbonized under carbon-neutral economies by injecting into geologic formations for either enhanced oil recovery or pure sequestration. Appraisal of environmental risk performance for geologic CO_2 storage (GCS) requires assessing the impact of the pore pressure increase and CO_2 saturation as a potential risk. Specifically, assessing this risk is required to ensure that the geologic storage systems perform in conformance with expectations and engineering tolerances. In this regard, many studies have investigated the behavior of these systems (Heath and McPherson, 2004; Shipton et al., 2004; Kim, 2008; Bachu and Celia, 2009; Nordbotten et al., 2009; Xiao et al., 2009; Carey et al., 2010; Bateman

et al., 2011; Celia and Nordbotten, 2011; Ellis et al., 2011; Bhowmik, 2012; Birkholzer et al., 2014, 2015; Singh and Srinivasan, 2014a, 2014b; Singh, 2014, 2017; Huerta et al., 2015; Oldenburg et al., 2016; Wolterbeek et al., 2016; Singh and Huerta, 2017; Singh and Islam, 2018). However, there is no study known to the author's knowledge that investigates the extent of pressure buildup and CO_2 plume saturation for different injection schemes that is constrained by the total amount of CO_2 injected. Out of the four injection schemes investigated here, only cyclic injection scheme, also known as huff-n-puff, has been investigated from the perspective of oil recovery in terms of the shut-in time (soaking time), injection rates, number of wells, etc (Song and Yang, 2013; Yu et al., 2016; Zuloaga et al., 2017; Fragoso et al., 2018).

This study investigates the spatio-temporal extent of pressure buildup and CO_2 saturation plume as a function of

four different injection schemes (i. constant rate, ii. stepwise increasing rate, iii. stepwise decreasing rate, and iv. cyclic rate) to understand how the variation in injection rate, by constraining the cumulative amount stored, affects the reservoir risk. The numerical metrics used to study the spatial-temporal extent of pressure buildup and CO_2 saturation plume are discussed under next section. In the results section, the spatio-temporal extent of pressure buildup and CO_2 saturation plume are obtained for four injection schemes, considering both homogeneous and heterogeneous geology of the site, and their implications on pure CO_2 storage and/or EOR are discussed. Finally, the study is summarized and conclusions are presented.

2. Method and approach

Generally, it is not possible to study the behavior of the pressure buildup and CO_2 plume evolution in most real reservoirs using analytical or semi-analytical solutions (Mathias et al., 2011; Bandilla et al., 2012; Mukhopadhyay et al., 2012; Mohamed, 2013; Yang et al., 2013) that assume the reservoir is homogeneous, ideal in geological structure, and of infinite size. These assumptions render their use for real reservoirs invalid, which are heterogeneous, non-ideal in geological structure, and are of finite size. Therefore, to study pressure buildup and CO_2 plume evolution in a realistic reservoir, we use the following two metrics (Bromhal et al., 2014) that are formulated mathematically here.

2.1 Spatio-temporal extent of pressure buildup and saturation

Two metrics that define the spatio-temporal extent of pressure buildup and CO_2 saturation plume, considered as important indicators of storage/risk relationships (Bromhal et al, 2014), were used in this study: i) the area of pressure buildup in the storage reservoir over time, and ii) the area of CO_2 saturation over time. Each is described in detail below.

2.1.1 Spatio-temporal extent of pressure buildup

Buildup in pressure can potentially drive CO_2 and/or brine out of a storage reservoir, which could impact ground water aquifers and other subsurface resources. Pressure buildup could also potentially cause increase in effective stress inside the storage site that can lead to seismic events. The evolution of the area of pressure buildup is a metric that suggests how a site's storage risks evolve over time.

For each scenario, ΔP was determined relative to the initial reservoir pressure prior to initiation of CO_2 injection. The spatio-temporal extent of pressure buildup is determined relative to four thresholds (Bromhal et al., 2014) for each site: 0.01 MPa, 0.1 MPa (a small but measurable pressure increase), 0.5 MPa, and 1.0 MPa (a threshold approximately sufficient to drive fluids from a storage reservoir to an above-zone aquifer for many scenarios). Even though these thresholds are useful as rule-of-thumb thresholds, real values will be site and case specific.

The behavior of this metric is explored by calculating an effective area of the pressure buildup ($A_{\Delta P}$), where $A_{\Delta P}$ is the projection onto the XY plane of the portion of the reservoir with a ΔP above a given threshold. First, spatial coordinates of the region inside a model are calculated where the differential pressure buildup is greater than a threshold pressure. A specific pressure buildup is the difference of pressure between its current state ($P[x, y, z, t]$) and the initial state ($P[x, y, z, 0]$):

$$\Delta P[x, y, z, t] = P[x, y, z, t] - P[x, y, z, 0] \qquad (1)$$

If region inside this domain where differential pressure buildup is greater than a specific threshold is represented as C_P, we can write:

$$C_P[x, y, z, t] = \begin{cases} 1 & when\ \Delta P[x, y, z, t] \geq \Delta P_{threshold} \\ 0 & otherwise \end{cases}$$
$$(2)$$

Now, the effective area of the pressure buildup is calculated by projecting this region represented by C_P on the XY plane and integrating it along the X and Y directions. Then, the projection of $C_P[x, y, z, t]$ to the XY plane, $proj_{C_P}[x, y, t]$, is given as follows:

$$proj_{C_P}[x, y, t] = \begin{cases} 1 & when\ C_P[x, y, z, t] > 0\ for\ any\ z \\ 0 & when\ C_P[x, y, z, t] = 0\ for\ all\ z \end{cases}$$
$$(3)$$

And the area of the pressure buildup, which will depend on the value of the pressure threshold, can be calculated as:

$$A_{\Delta P}[t] = \int_{x=-\infty}^{\infty} \int_{y=-\infty}^{\infty} proj_{C_P}[x, y, t] dy . dx \qquad (4)$$

For this work, this integral was estimated through a summation involving the discrete grid of a numerical reservoir model and using an early version of the REV tool (King, 2016) developed by the National Risk Assessment Partnership (NRAP).

2.1.2 Spatio-temporal extent of CO_2 saturation

Mobile free-phase CO_2 (above residual saturation) carries a potential risk of migrating outside of primary storage reservoir because of buoyant driving force. The evolution of the area of CO_2 saturation plume is another metric that suggests how a site's storage risks evolve over time, especially given the uncertainty in the critical threshold for mobility of free-phase CO_2.

The spatio-temporal extent of the CO_2 plume is considered relative to specific saturation thresholds, which in this work is determined relative to four CO_2 saturation thresholds for each site: 0.1 (irreducible CO_2 saturation that must be exceeded in a reservoir before the CO_2 phase becomes mobile), 0.3, 0.5, and 0.7 (maximum CO_2 saturation that can be present with residual water). The effective area of the CO_2 plume (A_s) was derived by projecting onto the XY plane the CO_2 plume with saturation above a certain threshold value, $S_{threshold}$. If S_{CO_2} is the saturation plume and the region where differential

saturation is greater than a specific threshold is represented as C_s, then we can write:

$$C_s[x, y, z, t] = \begin{cases} 1 & when \ S_{CO_2}[x, y, z, t] \geq S_{threshold} \\ 0 & otherwise \end{cases}$$

(5)

Now, the effective area of the saturation plume is calculated by projecting this region represented by C_s on the XY plane and integrating it along the X and Y directions. The projection of $C_s[x, y, z, t]$ to the XY plane, $proj_{C_s}[x, y, t]$, is given as following:

$$proj_{C_s}[x, y, t] = \begin{cases} 1 & when \ C_s[x, y, z, t] > 0 \ for \ any \ z \\ 0 & when \ C_s[x, y, z, t] = 0 \ for \ all \ z \end{cases}$$

(6)

And the CO_2 plume area above a threshold can be calculated as:

$$A_s[t] = \int_{x=-\infty}^{\infty} \int_{y=-\infty}^{\infty} proj_{C_s}[x, y, t] dy.dx$$

(7)

As with the area of saturation above, these values were numerically estimated using an early version of NRAP's REV tool.

2.2 Storage site

This study uses a representative model of a real site that is quite popular with the community studying CO_2 storage; a multi-layer sandstone with shale baffles as shown in Fig. 1. Although the geological structure used in this study is realistic, it is not the actual model of the site, therefore, we refer to this site shown in Fig. 1 as site-S. The site is deeper than 800 m, a minimum depth required for the CO_2 to exist in supercritical state (critical pressure 7.28 MPa and critical temperature 31.19 °C) because the hydrostatic pressure below 800 m is greater than the CO_2 critical pressure.

Examining the risk behavior of this site with four variations in injection rates, and constraining the cumulative amount stored, allows investigating how different injection schemes affect the likely extent of pressure buildup and CO_2 plume that impact the reservoir risk.

The dimensions of site-S are 640 m × 1.18 km along the xy-plane and its depth varies between 803 m and 1341 m, and having an uneven top surface with multiple structural highs. The geology of site-S constitutes a late-Miocene/early-Pliocene formation, overlain by clay-rich sediments and underlain by shaly sediments, which is represented by 51 simulation layers. Site-S is extremely permeable (permeability varying between 1 to 2 D) and the permeable layers are separated by thin layers of shale corresponding to mudstones. The thickness of the thin shale layers is typically 1 to 1.5 m and they extend laterally along the reservoir with baffles in the form of perforations. The permeability along the y-direction is similar to the permeability along the x-direction, whereas the permeability along z-direction is one-tenth of the values

along the x-direction. The porosity in site-S is assumed to be uniform (20%) throughout the volume of the reservoir.

The heterogeneity of the site is characterized using Dykstra-Parsons coefficient (Dykstra and Parsons, 1950), which is the most common measure used to characterize heterogeneity in the oil and gas industry (Jensen and Currie, 1990). Dykstra-Parsons coefficient (V_{dp}) is sometimes also referred to as coefficient of permeability variation and the definition of V_{dp} is given as follows:

$$V_{dp} = \frac{\ln(k)_{0.50} - \ln(k)_{0.16}}{\ln(k)_{0.50}}$$

(8)

Where, $k_{0.50}$ and $k_{0.16}$ are the median permeability value and permeability value at one standard deviation below median permeability, respectively. The minimum and maximum value of V_{dp} is 0 and 1, respectively, which represent homogeneous medium and "infinitely" (hypothetically) heterogeneous medium, respectively. Assuming that heterogeneous permeability (k) is log-normally distributed with mean μ and standard deviation σ, the above formulation of V_{dp} can be re-written as following:

$$V_{dp} = 1 - \exp(-\sigma), \ where \ \ln(k) \sim N(\mu, \sigma^2)$$

(9)

The robustness of V_{dp} as a heterogeneity measure lies in its assumption that the permeability data is log-normally distributed, which is actually true as many reservoirs have nearly log-normal permeability distributions (Jensen and Currie, 1990). The V_{dp} of permeability heterogeneity for site-S is 0.92.

### 2.2.1 Initial reservoir conditions and flow parameters

All the four injection schemes (constant rate, stepwise increasing rate, stepwise decreasing rate, and cyclic rate) assumed CO_2 injection over a period of 50 years followed by 250 years of post-injection observation period. Prior to initiation of CO_2 injection, hydrostatic equilibrium was established in the reservoir by enforcing zero mass flux at all side boundaries, and a gentle geothermal gradient (25 °C/km) was imposed along the vertical direction. The four variable injection schemes are shown in Fig. 2, where the total CO_2 injection over a period of 50 years for all the four injection schemes was 5 million tonnes.

The operating and initial reservoir conditions for this site are shown by Table 1.

We used experimental relative permeability of liquid CO_2 and water from Dempsey et al. (2014) who compiled experimental datasets from several sources (Bachu and Bennion, 2007; Perrin and Benson, 2009; Krevor et al., 2012; Berg et al., 2013) and used a best-fit curve (minimum mean squared error) through those datasets, as shown in Fig. 3. This best-fitted experimental relative permeability curve has an irreducible saturation of 0.3 and 0.1 for water and CO_2, respectively, endpoint relative permeability values of 0.8 and 1.0 for CO_2 and water, respectively, and exponent of 3.1 for both curves (Fig. 3).
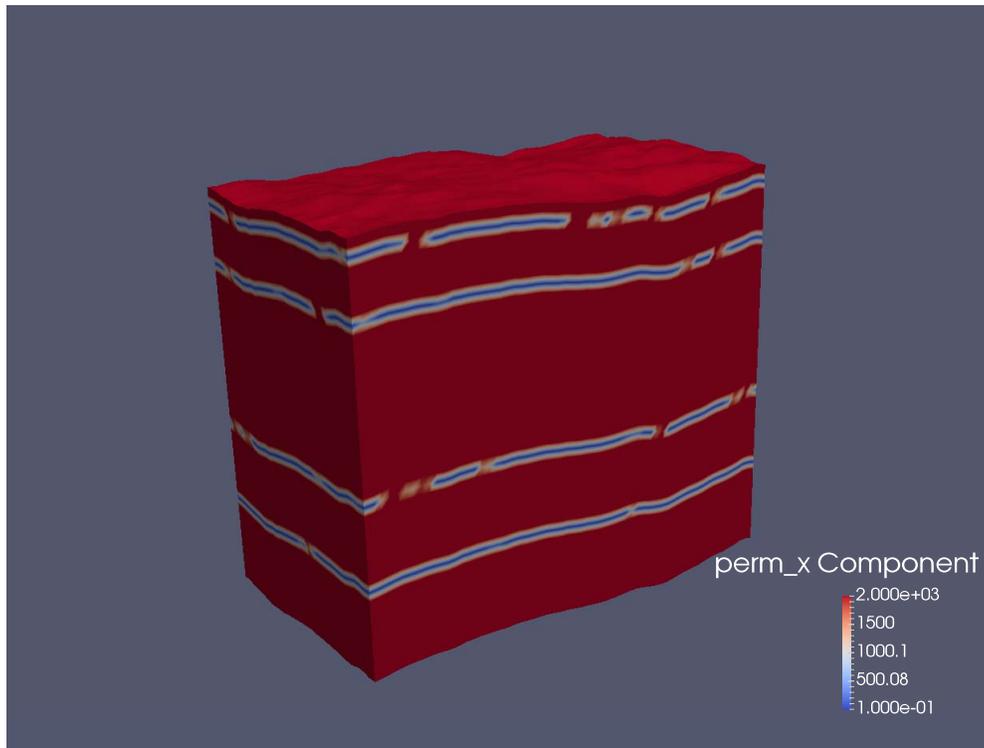
Fig. 1. Simulation model (exaggerated by a factor of 2 along z-axis) of Site-S depicting permeability (in mD) along x-direction (with arithmetic and geometric mean value of $\sim$ 1860 mD and 1026 mD). The blue layers are shale (extremely low permeability) with some baffles that may allow flow. Pore volume of both homogeneous and heterogeneous models are $\sim$ 75$\times$10^6 m^3. The V_{dp} of permeability heterogeneity is 0.92. The assumed permeability of a homogeneous scenario is 200 mD.
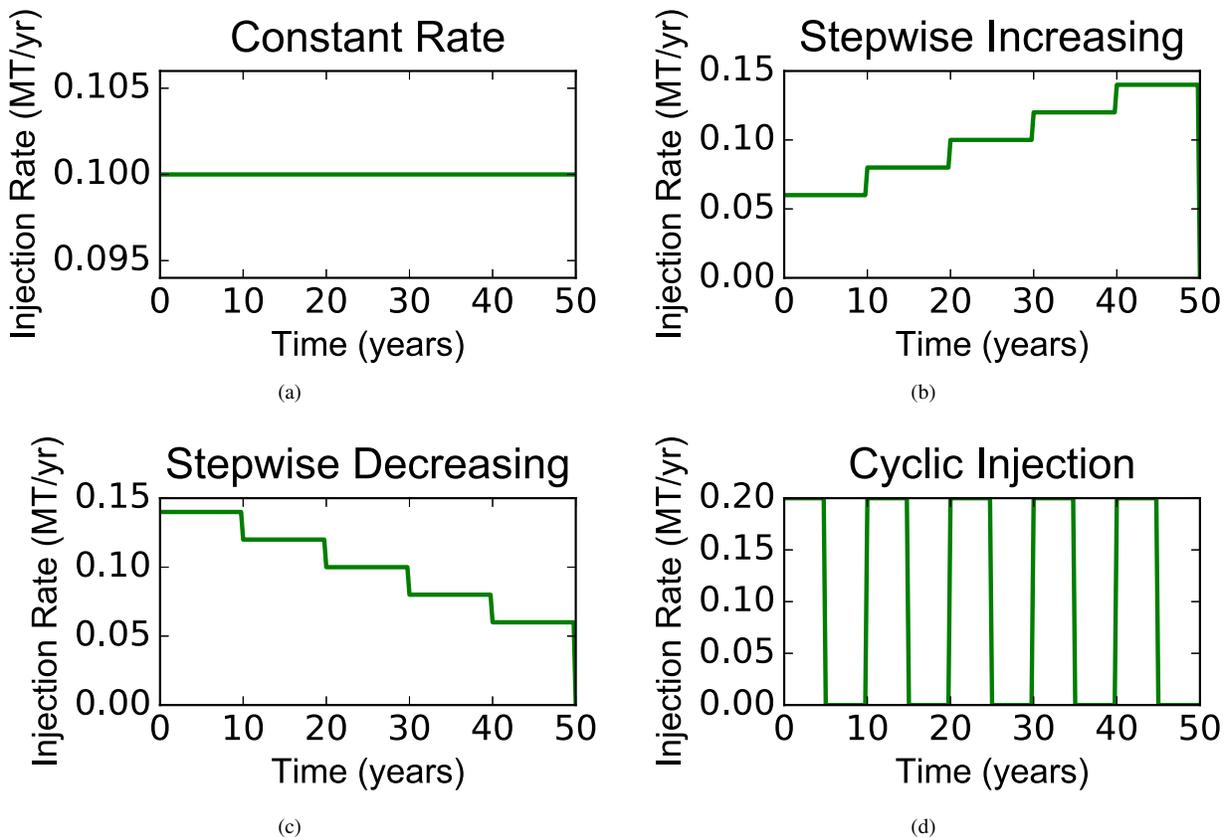
Fig. 2. Four different injection schemes (constant rate, stepwise increasing, stepwise decreasing, and cyclic injection, respectively) used in this study. The cumulative amount of CO_2 injected in all these four injection schemes is equal to 5 million tonnes.

Table 1. Reservoir operating and initial conditions.

Properties of site-S		Values
Areal dimension (km^2)	- -	0.64 × 1.18
Depth (m)	- -	803-1341
Pore volume (×10^6 m^3)	Homogeneous	75
	Heterogeneous	75
Initial pressure (MPa)	- -	10
Initial temperature (°C)	- -	40
Initial water saturation (%)	- -	100
Constant injection rate (MT/yr)	- -	0.1
Total injection (MT)	- -	5
Heterogeneity	Arithmetic mean porosity	0.2
	Arithmetic mean permeability (mD)	1860
	Geometric mean permeability (mD)	1026
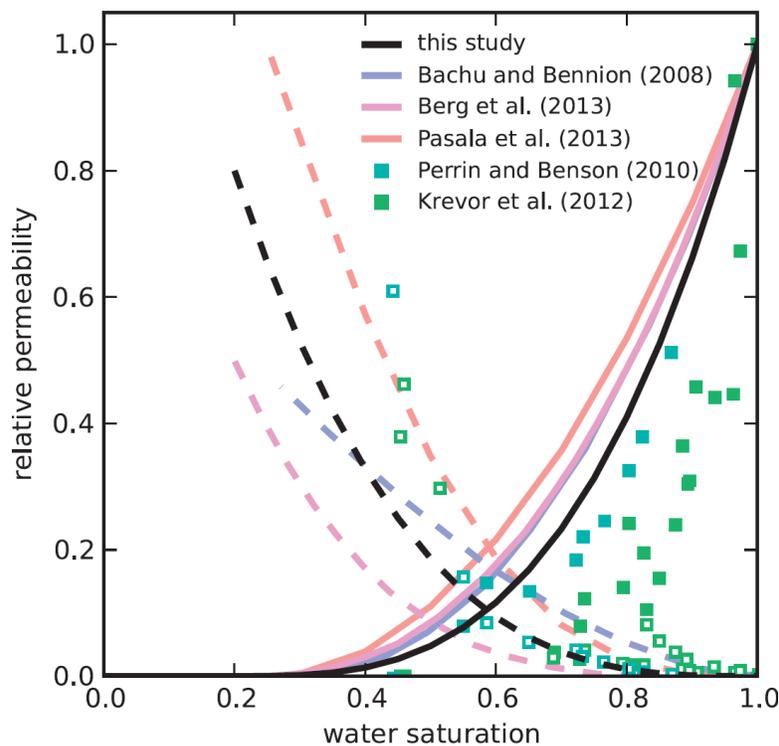
Fig. 3. Relative permeability curves (Dempsey et al., 2014) for supercritical CO_2 (dashed black curve) and water (solid black curve) used in this study. The experimentally-fitted relative permeability was used as a general representative of liquid CO_2 and water flow in this study.

2.2.2 Boundary conditions

Past studies for CO_2 storage related studies (e.g. Birkholzer and Zhou, 2009; Doughty, 2009; Zhou et al., 2009; Zhou and Birkholzer, 2011) have used Dirichlet (constant pressure/open flow) boundary conditions, including a benchmark study by Class et al. (2009) that assumes Dirichlet conditions equal to initial reservoir conditions for lateral boundaries and no-flow for the top and bottom boundaries. For this reason, this study assumes open-flow (Dirichlet) to brine and CO_2 across the four side boundaries and no-flow across the top and bottom boundaries to represent extensive and continuous shale sealing over and under each site.

The injector for site-S is located at the bottom layer of the reservoir and in the middle of the XY plane as a single node. Only one injector is placed in the middle to avoid the effects of pressure interference from multiple injectors that may distort the natural pattern of pressure evolution, and complicate interpretation of simulation results (e.g. Birkholzer and Zhou, 2009; Zhou and Birkholzer, 2011).
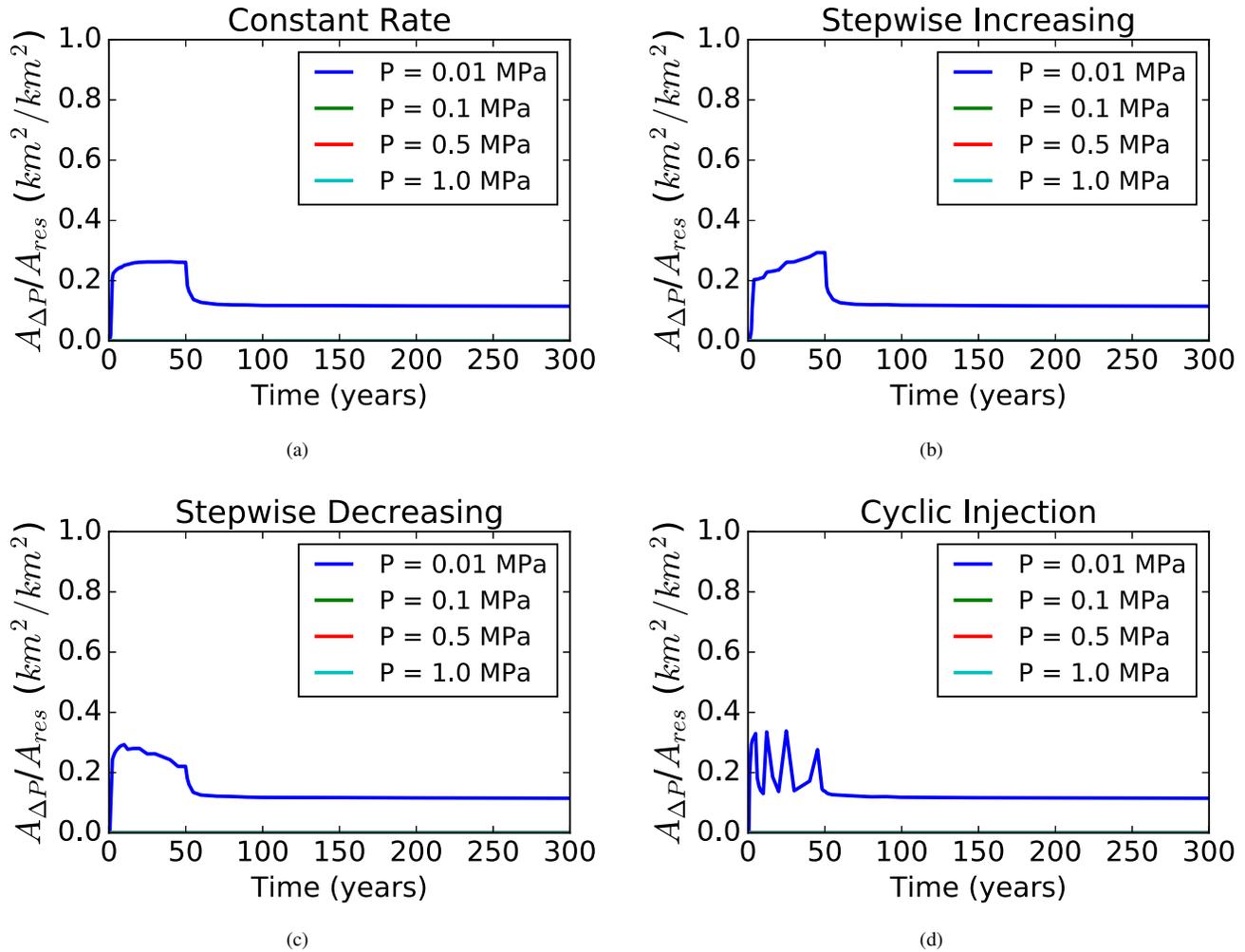
Fig. 4. $A_{\Delta P}(t)/A_{res}$ with constant, stepwise increasing, stepwise decreasing, and cyclic injection rates.

2.3 Numerical modeling description and simulation scenarios

Reservoir simulations were performed for two-phase, immiscible and non-isothermal flow of CO_2 and brine at the continuum scale without considering any chemical reactions and CO_2 dissolution in brine as these effects are unlikely to affect (Singh, 2017) the global behavior of the CO_2 at reservoir scale mainly because these effects are local in nature and their rate of mass transfer is quite slow (Kumar et al., 2005). Also, it is assumed that capillary pressure between supercritical CO_2 and brine is negligible, which is not an unrealistic assumption at field-scale with large pore sizes and the interfacial tension between CO_2 and brine that decreases with pressure (e.g. Alkan et al., 2010).

A finite-element heat and mass (FEHM) transfer simulator developed by Los Alamos National Laboratory was used to study the two-phase supercritical CO_2 and brine mixture in porous media. FEHM (Zyvoloski et al., 2011) solves heat and mass conservation equations for multi-phase, multi-fluid flow in porous media using an efficient, node-centered control volume implementation. Fluid properties of CO_2 are dynamically calculated in FEHM using spatial and temporal variation in pressure and temperature. CPU computational time to complete each simulation run using a single processor ranged up to 96 hours.

The evolution of pressure pulse and saturation plume in site-S was investigated for four injection schemes (constant rate, stepwise increasing rate, stepwise decreasing rate, and cyclic rate) using geological models considering: i) homogeneous and isotropic scenario, and ii) heterogeneous scenario. For the homogeneous and isotropic scenario, permeability and porosity were assumed to be 200 mD and 0.2, respectively, which results in similar pore volume (75×10^6 m^3) as that of heterogeneous geology.

3. Results and discussions

Spatio-temporal extent of pressure buildup and CO_2 saturation plume are computed for the site-S under two scenarios of homogeneous and heterogeneous geology, respectively. Results for these two metrics are obtained for the four injection schemes (constant rate, stepwise increasing rate, stepwise decreasing rate, and cyclic rate) while holding constant the
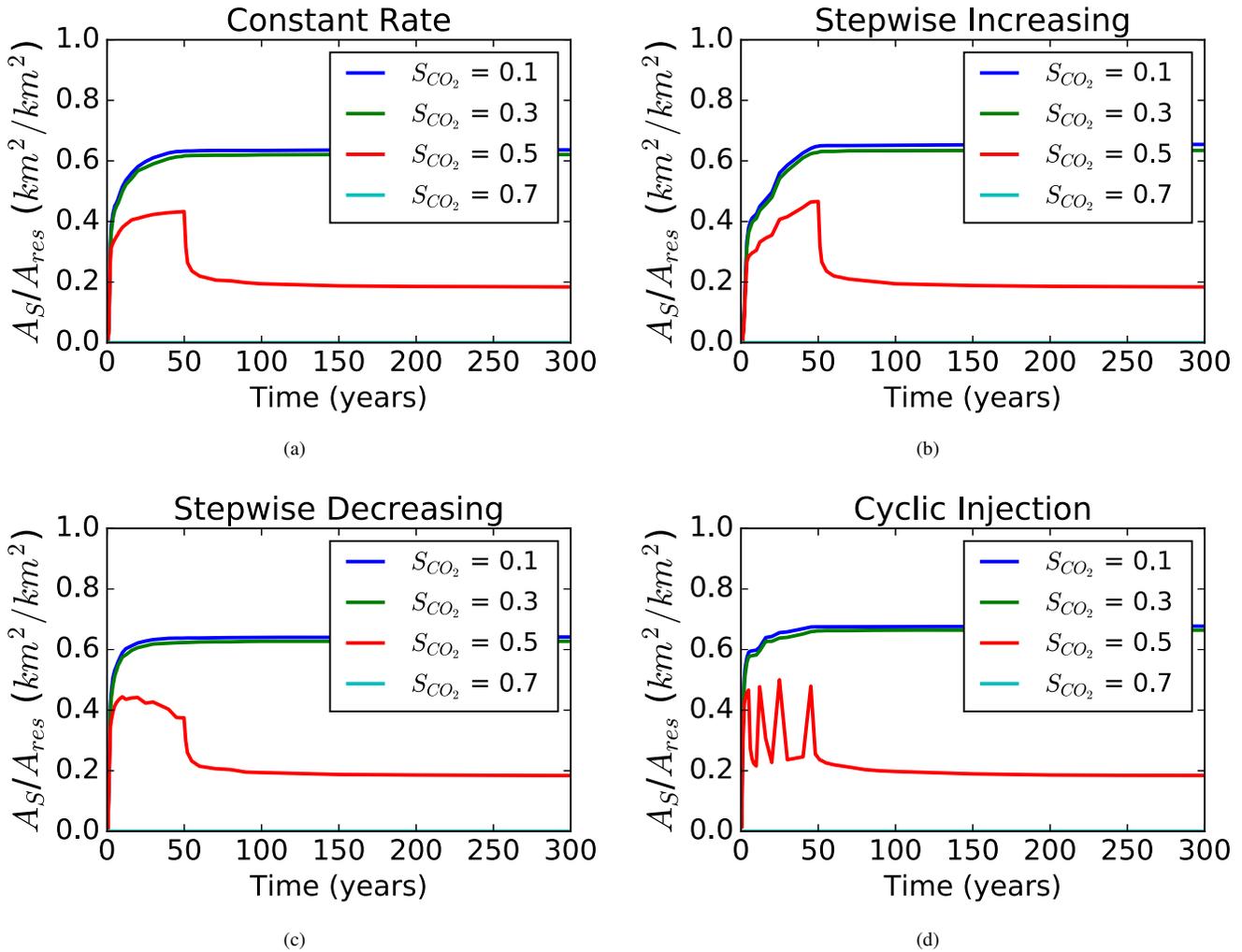
Fig. 5. $A_S(t)/A_{res}$ with constant, stepwise increasing, stepwise decreasing, and cyclic injection rates.

total amount of CO_2 injected. Dirichlet boundary condition (constant pressure/open flow) was used as it has been used by other studies (e.g. Birkholzer and Zhou, 2009; Class et al., 2009; Doughty, 2009; Zhou et al., 2009; Zhou and Birkholzer, 2011) that suggest it to be a realistic boundary condition for CO_2 storage studies.

3.1 With homogeneous model

Fig. 4 shows the areal extent of pressure buildup for the site with four different injection schemes considering geologically homogeneous case with four pressure thresholds ranging from 0.01 MPa to 1 MPa. Fig. 5 shows the areal extent of CO_2 saturation plume with four different injection schemes considering geologically homogeneous case with four saturation thresholds ranging from 0.1 to 0.7. The variation of pore pressure (normalized as $\frac{P-P_{min}}{P_{max}-P_{min}}$ to illustrate the variability due to < 1 MPa pressure buildup) with four injection schemes and comparison of normalized variation in both pressure and saturation are shown in section 3.1.2.

3.1.1 Spatio-temporal extent of pressure buildup and CO_2 plume

Except for the cyclic injections scheme, all other three injection schemes show a smooth variation in areal extent of pressure buildup and CO_2 saturation, while cyclic injection scheme introduces fluctuations in the areal extent of both pressure buildup and saturation. Although stepwise increasing and decreasing rates lead to subtle (very minute) wavering in the two variables plotted in Fig. 4 and Fig. 5, they are not significant. The extent of pressure buildup for $P > 0.01$ MPa was negligible, therefore, the three legends for $P = 0.1, 0.5, 1.0$ MPa are not visible in Fig. 4.

3.1.2 Variability in pressure buildup and saturation

Fig. 6 shows that cyclic injection tends to keep the pore pressure lower than the other three injection schemes, while the highest pressure increase over the entire injection period (50 years) is observed with stepwise decreasing rate. This figure also shows that the fluctuations in the cyclic injection rate are not transmitted to pore pressure for the entire cycle of the injection period. This is because of the compressibility
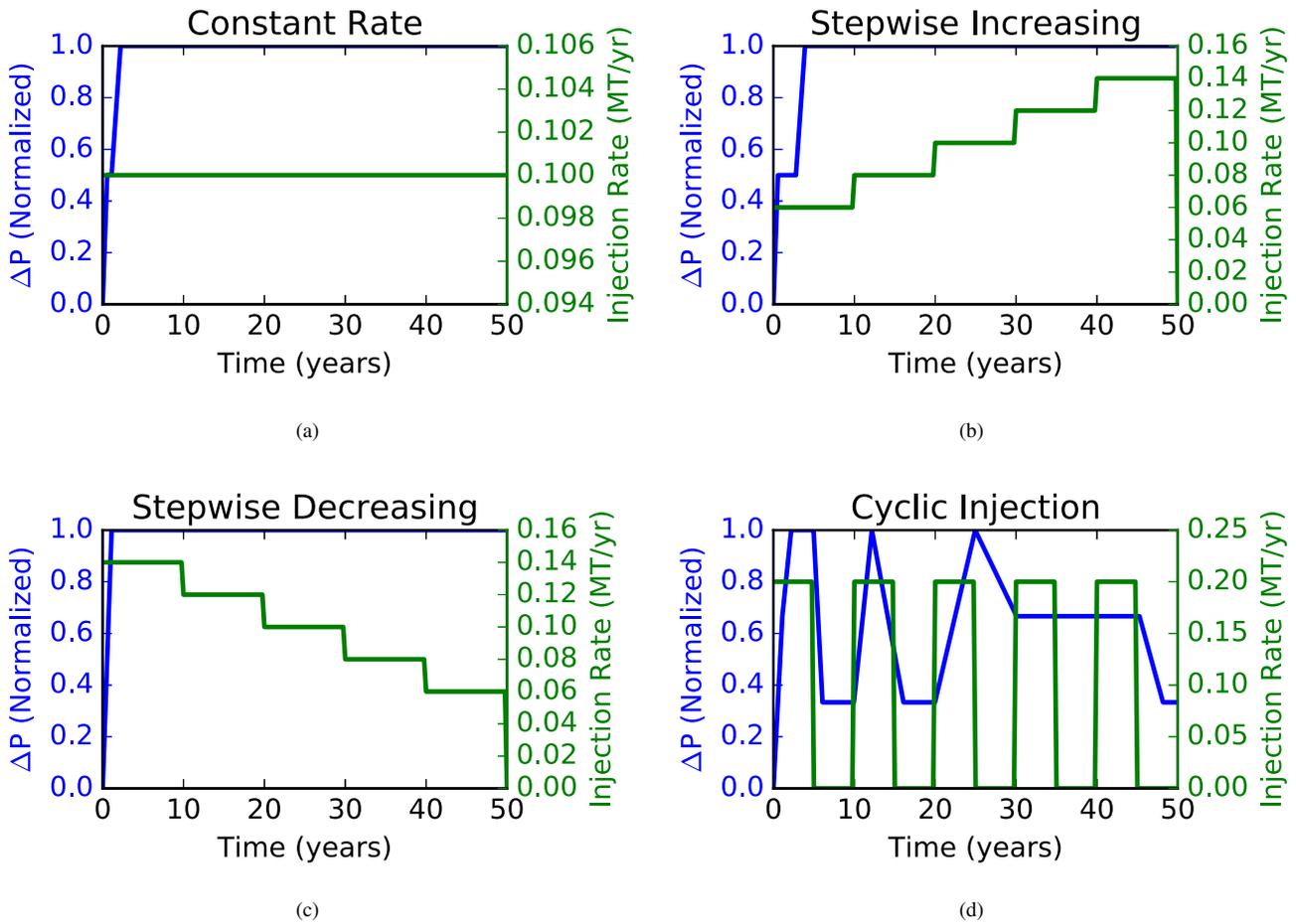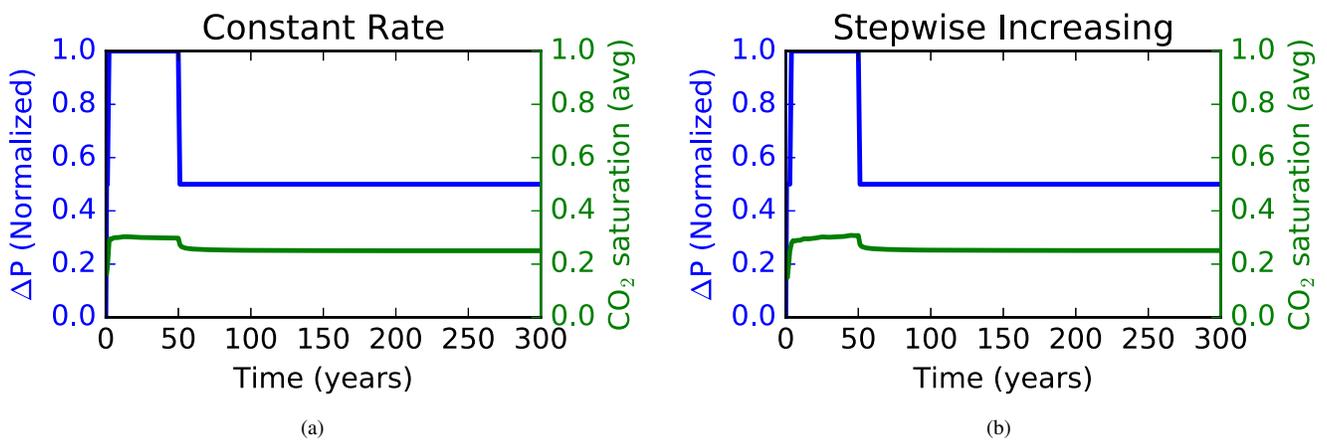
Fig. 6. Average pore pressure and injection rates with constant, stepwise increasing, stepwise decreasing, and cyclic injection rates.
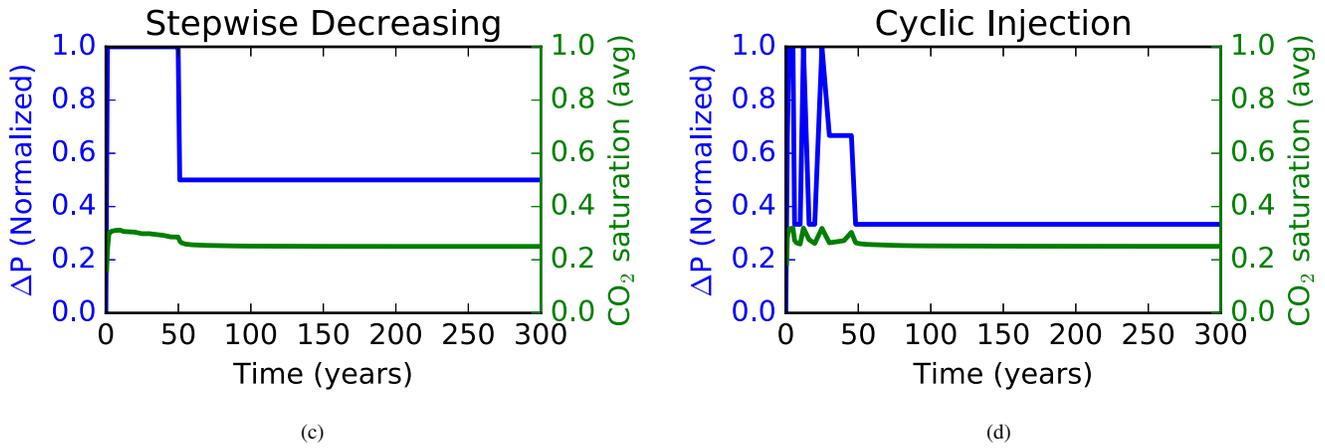
(c)

(d)

Fig. 7. Average pore pressure and average saturation with constant, stepwise increasing, stepwise decreasing, and cyclic injection rates.

of CO_2 attenuates the impact of fluctuating injection rates that results in dampening the pressure.

Fig. 7 shows that the normalized CO_2 saturation follows the behavior of the pressure increase, i.e., the stepwise decreasing rate maintains the highest CO_2 saturation value over the entire injection period, and the cyclic fluctuations in the pressure (for cyclic injection rate) are also mimicked by the CO_2 saturation, although the fluctuations in the saturation are not as pronounced as the fluctuations in pressure (Fig. 7).

3.2 With heterogeneous model

Fig. 8 shows the areal extent of pressure buildup for the site with four different injection schemes considering geologically homogeneous case with four pressure thresholds ranging from 0.01 MPa to 1 MPa. Fig. 9 shows the areal extent of CO_2 saturation plume with four different injection schemes considering geologically homogeneous case with four saturation thresholds ranging from 0.1 to 0.7. The variation of pore pressure (normalized to illustrate the variability) with four injection schemes and comparison of variation in both pressure and saturation are shown in section 3.2.2.

3.2.1 Spatio-temporal extent of pressure buildup and CO_2 plume

Heterogeneous scenario of site-S does not seem to affect the results of spatio-temporal extent of pressure buildup and saturation as shown in Fig. 8 and Fig. 9. Cyclic injection scheme introduces fluctuations in the areal extent of both pressure buildup and saturation, while other three injection schemes show a smooth variation in areal extent of pressure buildup and CO_2 saturation. The extent of pressure buildup for $P > 0.01$ MPa was negligible, therefore, the three legends for $P = 0.1, 0.5, 1.0$ MPa are not visible in Fig. 8.

3.2.2 Variability in pressure buildup and saturation

The results shown in Fig. 10 and Fig. 11 follow exactly the same behavior as observed under homogeneous case, with small differences introduced as a result of heterogeneity. For example in Fig. 10, the results for stepwise increasing and stepwise decreasing injection schemes also show some fluctuations with time that were not present in the case of homogeneous geology. These fluctuations in the case of stepwise increasing and stepwise decreasing injection schemes
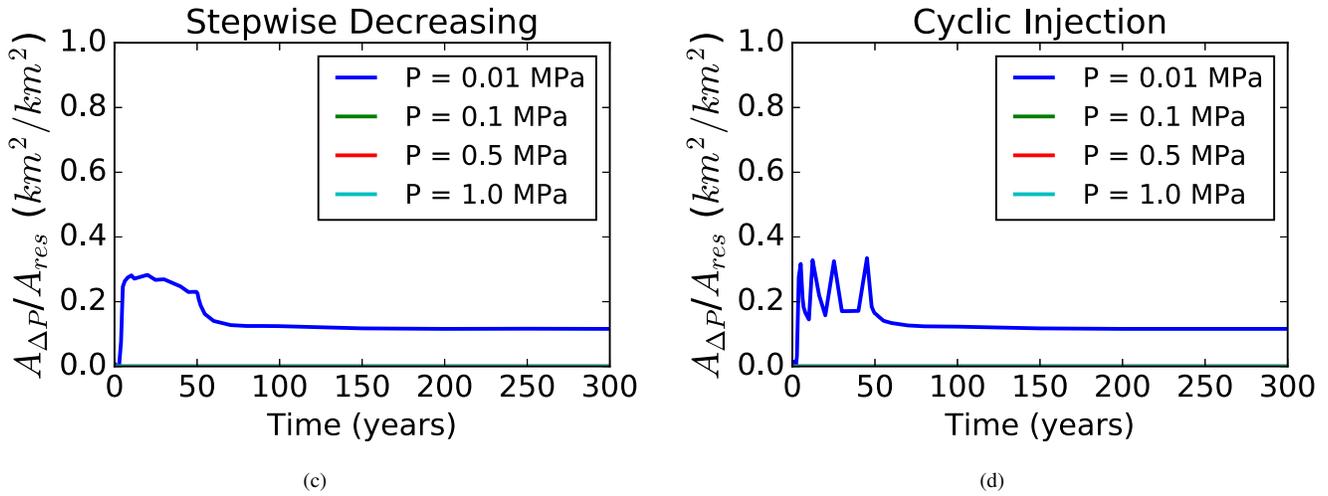

(a)

(b)
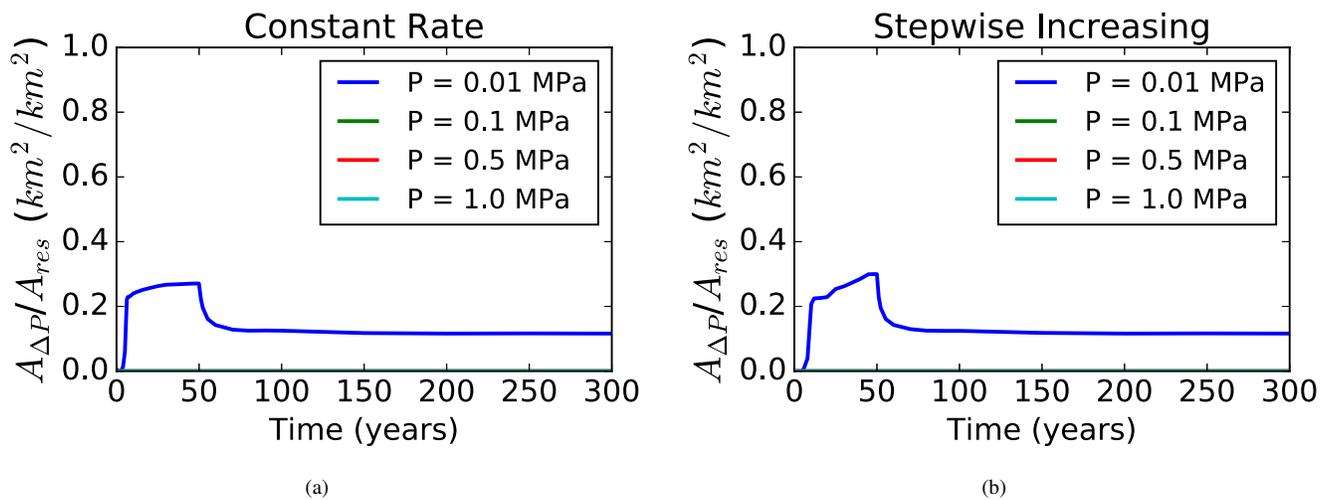
Fig. 8. $A_{\Delta P}(t)/A_{res}$ with constant, stepwise increasing, stepwise decreasing, and cyclic injection rates.
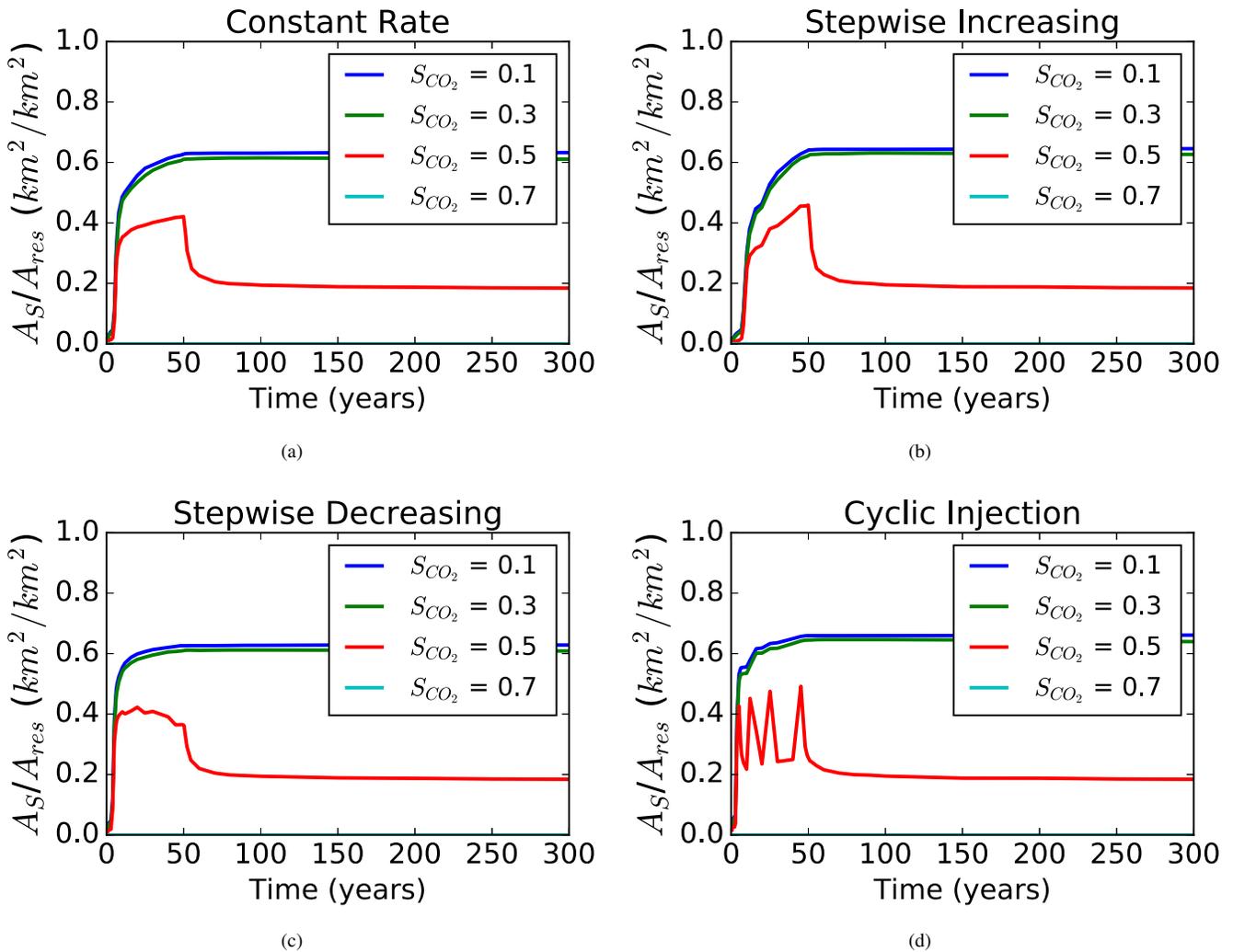

Fig. 9. $A_S(t)/A_{res}$ with constant, stepwise increasing, stepwise decreasing, and cyclic injection rates.
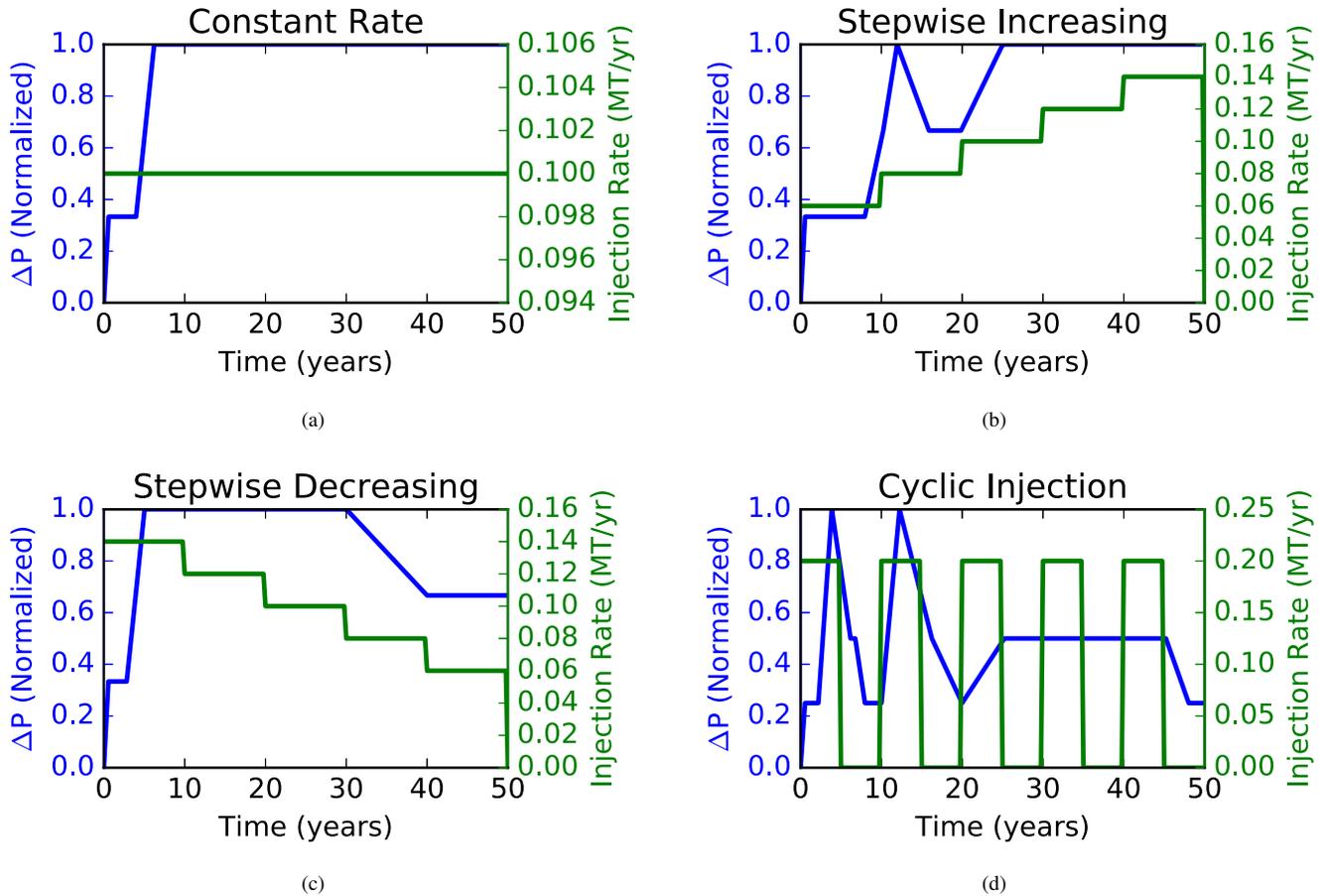
Fig. 10. Average pore pressure and injection rates with constant, stepwise increasing, stepwise decreasing, and cyclic injection rates.

are possibly introduced due to lateral shale layers with discontinuities in the form of perforations/baffles that stops the CO_2, but an increase or decrease in injection rate changes the local pressure gradient that allows the CO_2 to move towards the baffles and then rise above due to buoyancy. However, these moderate fluctuations in pore pressure introduced by stepwise increasing and stepwise decreasing injection schemes are not observed in the saturation plume as shown by Fig. 11.

3.3 Effect of boundary conditions

The pressure buildup with the open-flow boundary condition (allowing both the CO_2 and brine to flow out freely through initial reservoir pressure) is not very large ($<$ 1 MPa), but the magnitude of pressure buildup increases with the increase in flow region's boundaries. This observation has been discussed by other studies (Doughty, 2009; Zhang et al., 2016), which reported that location of the boundary (flow region of the reservoir) relative to plume extent can have a very significant contribution on pressure buildup on CO_2 injection. However, boundaries do not play an important role if the flow region of the model is large for the pressure perturbation to reach its boundaries (e.g. Birkholzer and Zhou, 2009; Doughty, 2009; Zhou et al., 2009; Smith et al., 2011; Zhou and Birkholzer, 2011; Schäfer et al., 2012; Zhang et

al., 2016). Closed boundary conditions are expected to result in general (average) pressure increase in the storage system, while in comparison open-flow boundaries are less susceptible to pressure increase except if there are multiple injectors that can cause pressure interference (e.g. Birkholzer and Zhou, 2009; Zhou and Birkholzer, 2011) depending on the spacing of the wells and the reservoir size.

4. Summary and conclusions

This study investigated the spatio-temporal extent of pressure buildup and CO_2 saturation plume as a function of four different injection schemes (constant rate, stepwise increasing rate, stepwise decreasing rate, and cyclic rate) to understand how the variation in injection rate, by constraining the cumulative amount stored, affects the reservoir risk. Spatio-temporal extent of pressure buildup and CO_2 saturation plume were obtained for four injection schemes, considering both homogeneous and heterogeneous geology of the site. Results showed that cyclic injection tends to keep the pore pressure lower than the other three injection schemes, while the highest pressure increase over the entire injection period (50 years) is observed with stepwise decreasing rate. The compressibility of CO_2 plays a role in attenuating the impact of fluctuating cyclic injection signals on pressure after 30 years of injection,
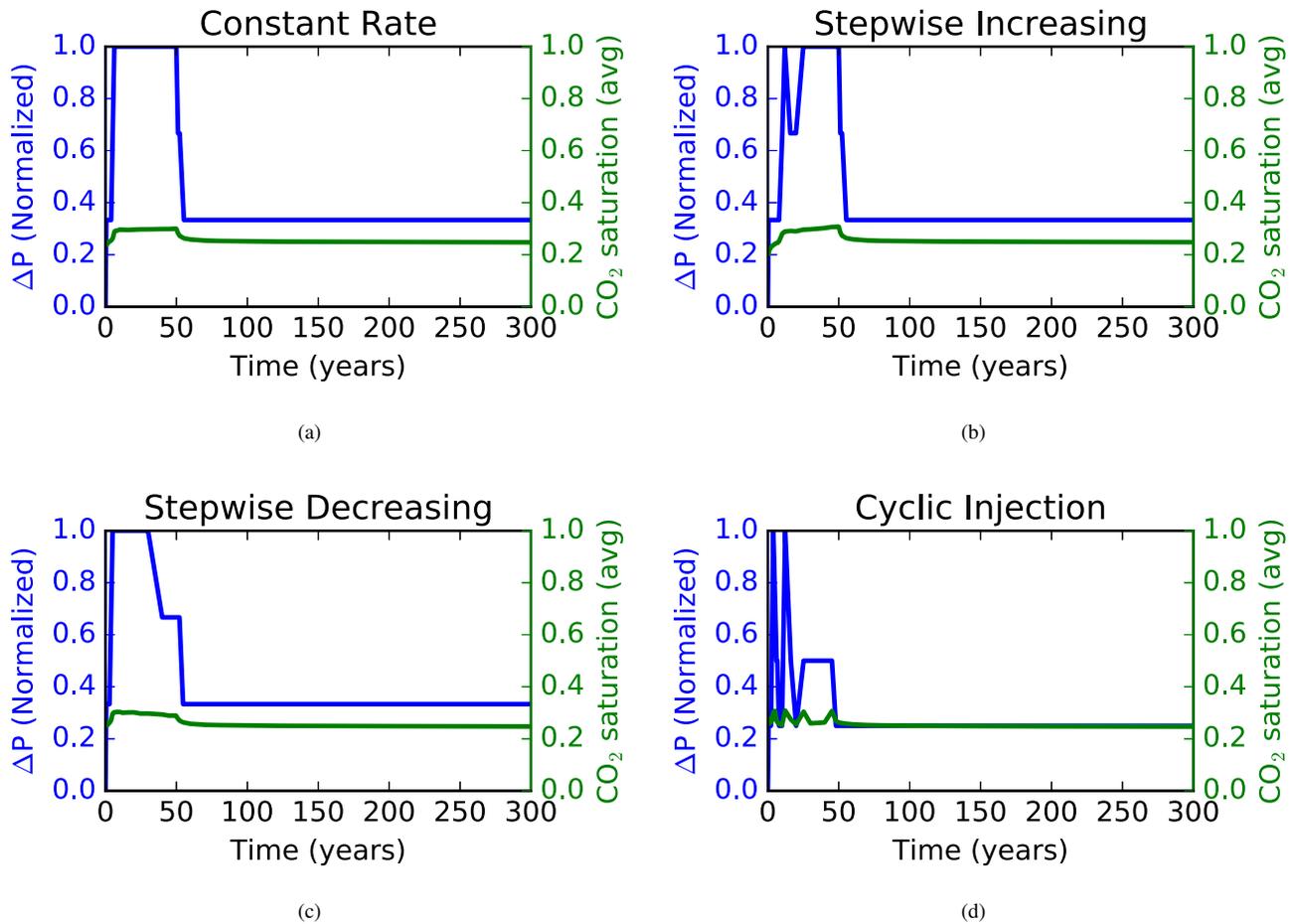
Fig. 11. Average pore pressure and average saturation with constant, stepwise increasing, stepwise decreasing, and cyclic injection rates.

where this time decreases by 5 years in case of heterogeneous scenario. Although cyclic fluctuations in the pressure (by cyclic injection rate) are also mimicked by the CO_2 saturation, they are not as pronounced as the fluctuations in pressure. Layered heterogeneity of the model introduces small differences compared to the homogeneous case in a way that stepwise increasing and stepwise decreasing injection schemes also show some fluctuations in pore pressure with time, but these fluctuations are not observed in the saturation plume. However, layered heterogeneity of site-S did not affect the areal extent of the pressure buildup or the saturation.

These results have important implications for storage reservoirs that may be prone to high pressure buildup during injection because of their geology, for instance fractured shale reservoirs (Myshakin et al., 2018; Singh and Cai, 2018), such that it would be preferable to store CO_2 using a cyclic injection scheme that will keep the pore pressure lower than the other three injection schemes. These results also carry important implications for enhanced oil recovery (EOR) using CO_2 where the primary goal is to drive the oil out by increasing pore pressure; for EOR by CO_2, stepwise decreasing rate would be most preferable as it leads to highest increase in pore pressure.

It has been shown in the context of oil recovery (Song and

Yang, 2013; Yu et al., 2016) by huff-n-puff, which mimics a cyclic injection, shut-in time does not have any effect on the oil recovery except that the short shut-in time (or soaking time) recovers the oil faster. In the context of pressure buildup, it is apparent from Fig. 6 and 10 that a shorter shut-in time (or soaking period) for the cyclic injection may lead to a lower drop in the pressure built up during injection and a larger shut-in time may lead to a larger drop in the pressure built up during injection.

Acknowledgments

References

Bachu, S., Bennion, B. Effects of in-situ conditions on relative permeability characteristics of CO_2-brine systems. Environ. Geol. 2008, 54(8): 1707-1722.

Bachu, S., Celia, M.A. Assessing the potential for CO_2 leakage, particularly through wells, from geological storage sites. Carbon Sequestration and Its Role in the Global Carbon Cycle 2009, 183: 203-216.

Bandilla, K.W., Kraemer, S.R., Birkholzer, J.T. Using semi-analytic solutions to approximate the area of potential impact for carbon dioxide injection. Int. J. Greenh. Gas Con. 2012, 8: 196-204.

Bateman, K., Rochelle, C., Lacinska, A., et al. CO_2-porewater-rock reactions-Large-scale column experiment (Big Rig II). Energy Procedia 2011, 4: 4937-4944.

Berg, S., Oedai, S., Ott, H. Displacement and mass transfer between saturated and unsaturated CO_2-brine systems in sandstone. Int. J. Greenh. Gas Con. 2013, 12: 478-492.

Bhowmik, S. Predicting the migration of CO_2 plume in saline aquifers using probabilistic history matching approaches. University of Texas at Austin, USA, 2012.

Birkholzer, J., Cihan, A., Bandilla, K. A tiered areaofreview framework for geologic carbon sequestration. Greenh. Gases 2014, 4(1): 20-35.

Birkholzer, J.T., Oldenburg, C.M., Zhou, Q. CO_2 migration and pressure evolution in deep saline aquifers. Int. J. Greenh. Gas Con. 2015, 40: 203-220.

Bromhal, G., ArcentalesBastidas, D., Birkholzer, J., et al. Use of science-based prediction to characterize reservoir behavior as a function of injection characteristics, geological variables, and time. NRAP-TRS-I-005-2014, Department of Energy, National Energy Technology Laboratory, USA, 2014.

Carey, J.W., Svec, R., Grigg, R., et al. Experimental investigation of wellbore integrity and CO_2-brine flow along the casing-cement microannulus. Int. J. Greenh. Gas Con. 2010, 4(2): 272-282.

Celia, M.A., Nordbotten, J.M. How simple can we make models for CO_2 injection, migration, and leakage? Energy Procedia 2011, 4: 3857-3864.

Dempsey, D., Kelkar, S., Pawar, R., et al. Modeling caprock bending stresses and their potential for induced seismicity during CO_2 injection. Int. J. Greenh. Gas Con. 2014, 22: 223-236.

Doughty, C. Investigation of CO_2 plume behavior for a large-scale pilot test of geologic carbon storage in a saline formation. Transport Porous Med. 2010, 82(1): 49-76.

Dykstra, H., Parsons, R.L. The prediction of oil recovery by waterflood. Secondary Recovery of Oil in the United States 1950, 2: 160-174.

Ellis, B., Peters, C., Fitts, J., et al. Deterioration of a fractured carbonate caprock exposed to CO_2-acidified brine flow. Greenh. Gases 2011, 1(3): 248-260.

Fragoso, A., Selvan, K., Aguilera, R. Breaking a paradigm: Can oil recovery from shales be larger than oil recovery from conventional reservoirs? The answer is yes! Paper SPE189784 Presented at the SPE Canada Unconventional Resources Conference, Calgary, Alberta, Canada, 13-14 March, 2018.

Heath, J.E., McPherson, B.J. 2-D numerical modeling of a fault zone leaking carbon dioxide in east central Utah. Paper AGU Presented at Fall Meeting Abstracts, 2004.

Huerta, N.J., Hesse, M.A., Bryant, S.L., et al. Reactive transport of CO_2-saturated water in a cement fracture: Application to wellbore leakage during geologic CO_2 storage. Int. J. Greenh. Gas Con. 2016, 44: 276-289.

Jensen, J.L., Currie, I.D. A new method for estimating the Dykstra-Parsons coefficient to characterize reservoir heterogeneity. SPE Reserv. Eng. 1990, 5(3): 369-374.

Kim, D. Scale-up of reactive flow through network flow modeling. The Graduate School, Stony Brook University: Stony Brook, NY, USA, 2008.

King, S. Reservoir Evaluation and Visualization (REV) Tool Users Manual, Version: 2016.11-1.2.0. U.S. Department of Energy, National Energy Technology Laboratory, 2016.

Krevor, S.C.M., Pini, R., Zuo, L., et al. Relative permeability and trapping of CO_2 and water in sandstone rocks at reservoir conditions. Water Resour. Res. 2012, 48(2): W02532.

Kumar, A., Noh, M.H., Ozah, R.C., et al. Reservoir simulation of CO_2 storage in aquifers. SPE J. 2005, 10(3): 336-348.

Mathias, S.A., De Miguel, G.J.G.M., Thatcher, K.E., et al. Pressure buildup during CO_2 injection into a closed brine aquifer. Transport Porous Med. 2011, 89(3): 383-397.

Mohamed, A.M.A.S. Semi-analytical solution for multiphase fluid flow applied to CO_2 sequestration in geologic porous media. Texas A&M University, USA, 2013.

Mukhopadhyay, S., Yang, S.Y., Yeh, H.D. Pressure buildup during supercritical carbon dioxide injection from a partially penetrating borehole into gas reservoirs. Transport Porous Med. 2012, 91(3): 889-911.

Myshakin, E.M., Singh, H., Sanguinito, S., et al. Numerical estimations of storage efficiency for the prospective CO_2 storage resource of shales. Int. J. Greenh. Gas Con. 2018, 76: 24-31.

Nordbotten, J.M., Kavetski, D., Celia, M.A., et al. Model for CO_2 leakage including multiple geological layers and multiple leaky wells. Environ. Sci. Technol. 2008, 43(3): 743-749.

Oldenburg, C.M., Cihan, A., Zhou, Q., et al. Geologic carbon sequestration injection wells in overpressured storage reservoirs: Estimating area of review. Greenh. Gases 2016, 6(6): 775-786.

Perrin, J.C., Benson, S. An experimental study on the influence of sub-core scale heterogeneities on CO_2 distribution in reservoir rocks. Transport Porous Med. 2010, 82(1): 93-109.

Shipton, Z.K., Evans, J.P., Kirschner, D., et al. Analysis of CO_2 leakage through 'low-permeability' faults from natural reservoirs in the Colorado Plateau, east-central Utah. Geological Society, London, Special Publications 2004, 233(1): 43-58.

Singh, H. Scale-up of reactive processes in heterogeneous media. University of Texas at Austin, USA, 2014.

Singh, H. Representative elementary volume (REV) in spatio-temporal domain: A method to find REV for dynamic pores. J. Earth Sci-China 2017, 28(2): 391-403.

Singh, H., Cai, J. Screening improved recovery methods in tight-oil formations by injecting and producing through fractures. Int. J. Heat Mass Tran. 2018, 116: 977-993.

Singh, H., Huerta, N.J. Detecting subsurface fluid leaks in real-time using injection and production rates. Adv. Water Resour. 2017, 110: 147-165.

Singh, H., Islam, A. Enhanced safety of geologic CO_2 storage with nanoparticles. Int. J. Heat Mass Tran. 2018, 121: 463-476.

Singh, H., Srinivasan, S. Scale up of reactive processes in heterogeneous media-numerical experiments and semi-analytical modeling. Paper SPE169133 Presented at the SPE Improved Oil Recovery Symposium, Tulsa, Oklahoma, USA, 12-16 April, 2014a.

Singh, H., Srinivasan, S. Some perspectives on scale-up of flow and transport in heterogeneous media. Bull. Can. Pet. Geol. 2014b.

Song, C., Yang, D. Performance evaluation of CO_2 huff-n-puff processes in tight oil formations. Paper SPE167217 Presented at the SPE Unconventional Resources Conference Canada, Calgary, Alberta, Canada, 5-7 November, 2013.

Wolterbeek, T.K.T., Peach, C.J., Raoof, A., et al. Reactive transport of CO_2-rich fluids in simulated wellbore interfaces: Flow-through experiments on the 1-6 m length scale. Int. J. Greenh. Gas Con. 2016, 54: 96-116.

Xiao, Y., Xu, T., Pruess, K. The effects of gas-fluid-rock interactions on CO_2 injection and storage: Insights from reactive transport modeling. Energy Procedia 2009, 1(1): 1783-1790.

Yang, Z., Niemi, A., Tian, L., et al. Modelling of far-field pressure plumes for carbon dioxide sequestration. Energy Procedia 2013, 40: 472-480.

Yu, Y., Li, L., Sheng, J.J. Further discuss the roles of soaking time and pressure depletion rate in gas huff-n-puff process in fractured liquid-rich shale reservoirs. Paper SPE181471 Presented at the SPE Annual Technical Conference and Exhibition, Dubai, UAE, 26-28 September, 2016.

Zhang, L., Dilmore, R.M., Bromhal, G.S. Effect of outer boundary condition, reservoir size, and CO_2 effective permeability on pressure and CO_2 saturation predictions under carbon sequestration conditions. Greenh. Gases 2016, 6(4): 546-560.

Zuloaga, P., Yu, W., Miao, J. et al. Performance evaluation of CO_2 Huff-n-Puff and continuous CO_2 injection in tight oil reservoirs. Energy 2017, 134: 181-192.

Zyvoloski, G.A., Robinson, B.A., Dash, Z.V., et al. Summary of the models and methods for the FEHM application-a finite-element heat-and mass-transfer code. No. LA–13307-MS, Los Alamos National Laboratory, 1997.